

Domain Transfer in Latent Space (DTLS) Wins on Image Super-Resolution – a Non-Denoising Model

Chun-Chuen Hui^{1,2}

Wan-Chi Siu^{1,2}

Ngai-Fong Law²

¹Caritas Institute of Higher Education

²The Hong Kong Polytechnic University

cchui@cihe.edu.hk enwcsiu@polyu.edu.hk ngai.fong.law@polyu.edu.hk

Abstract

Large scale image super-resolution is a challenging computer vision task, since vast information is missing in a highly degraded image, say for example for scale $\times 16$ super-resolution. Diffusion models are used successfully in recent years in extreme super-resolution applications, in which Gaussian noise is used as a means to form a latent photo-realistic space, and acts as a link between the space of latent vectors and the latent photo-realistic space. There are quite a few sophisticated mathematical derivations on mapping the statistics of Gaussian noises making Diffusion Models successful. In this paper we propose a simple approach which gets away from using Gaussian noise but adopts some basic structures of diffusion models for efficient image super-resolution. Essentially, we propose a DNN to perform domain transfer between neighbor domains, which can learn the differences in statistical properties to facilitate gradual interpolation with results of reasonable quality. Further quality improvement is achieved by conditioning the domain transfer with reference to the input LR image. Experimental results show that our method outperforms not only state-of-the-art large scale super resolution models, but also the current diffusion models for image super-resolution. The approach can readily be extended to other image-to-image tasks, such as image enlightening, inpainting, denoising, etc.

1. Introduction

Diffusion models have rapidly advanced image synthesis in recent years, achieving outstanding performance [4, 5, 11, 12, 14, 24–26, 28, 29, 32, 35, 38]. Denoising Diffusion Probabilistic Model (DDPM) [9] was firstly proposed to generate images by reversing a Markovian process. This is to remove Gaussian noises gradually from a latent pattern via a learned noise prediction network, typically U-Net [11, 26] or U-ViT adopted in [2].

Figure 1a shows the training procedure of the DDPM. To train the U-Net in DDPM, an input image x_0 (where 0 indicates $t=0$, in the noiseless domain) is added with noise N according to timestep t , which is randomly drawn from 1 to

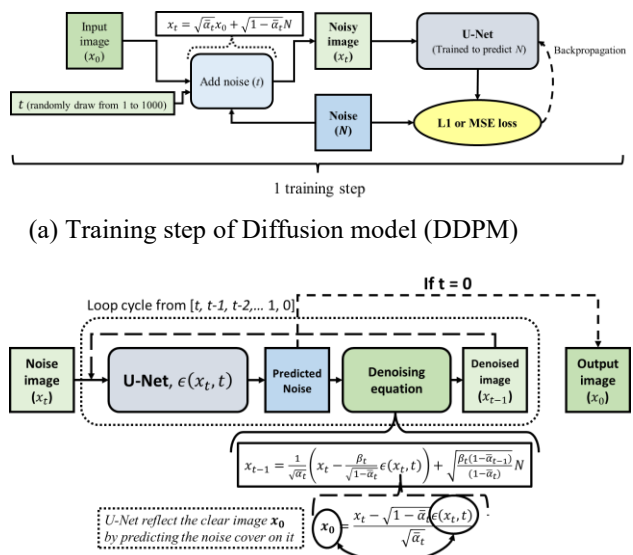


Figure 1. Training and image generation flow of DDPM

1000. The noise adding process follows eqn.1 with scaling $\sqrt{\bar{\alpha}_t}$ as shown below,

$$x_t = \sqrt{\bar{\alpha}_t}x_0 + \sqrt{1 - \bar{\alpha}_t}N \quad (1)$$

The noisy image x_t is inputted into the U-Net model to predict the noise N added to x_0 , where the prediction is used to calculate the loss for image generation. Mean absolute error (L1 loss) or mean square error (MSE loss) can be used as a loss function in the training procedure. By this training structure, the U-Net can learn the statistical properties of the image dataset, $\{x_0\}$, in training. Note that the training and generation procedures can identify image distributions from different timesteps t , since the training is generalized by using random timesteps.

For the generation process as shown in Fig. 1b, a noisy image x_t is inputted into a loop cycle. In the loop, the trained U-Net firstly produces a noise pattern for x_t . The predicted noise pattern is then processed with a denoising equation and the denoised image x_{t-1} is then outputted. The denoised image x_{t-1} goes back to the beginning of the loop and to

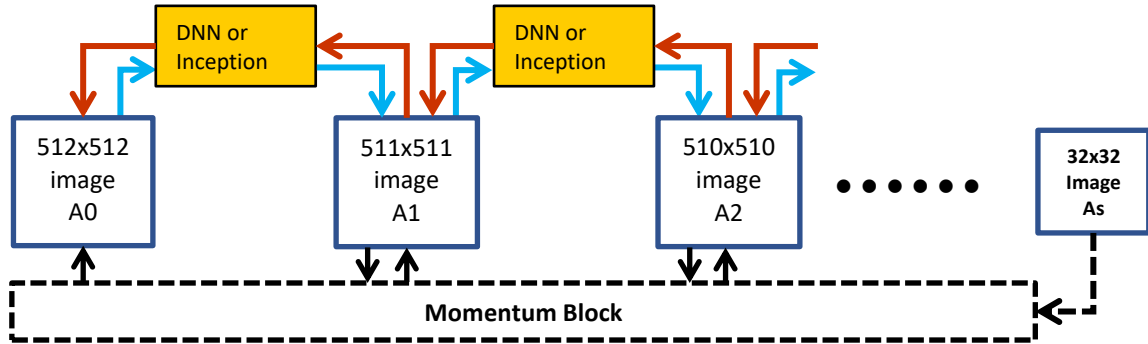


Figure 2. Conceptual idea of our model

make denoising again with the U-Net again until $t=0$. At $t=0$, the prediction of the U-Net is supposed noiseless, thus, the denoising equation is no longer employed. This last prediction result becomes the output i.e., image x_0 .

Note that in DDPM, the denoise equation can usually expressed as,

$$x_{t-1} = \frac{1}{\sqrt{\alpha_t}} \left(x_t - \frac{\beta_t}{\sqrt{1-\alpha_t}} \epsilon(x_t, t) \right) + \sqrt{\frac{\beta_t(1-\alpha_{t-1})}{(1-\alpha_t)}} N(0,1) \quad (2)$$

where $\epsilon(x_t, t)$ represents the output from learnt U-Net, and is used to predict noise. We want to clarify that although the U-Net is predicting the noise pattern, it is statistically linked to the possible noiseless image x_0 . By reverting equation 1, we can obtain,

$$x_0 = (x_t - \sqrt{1-\alpha_t} N) / \sqrt{\alpha_t} \quad (3)$$

This means that the predicted noise image always refers to the latent real image representation of x_0 . The diffusion model makes use of the trained U-Net to predict hidden clean image x_0 and makes use of the denoising equation to guide the transformation process from latent space to photo-realistic space. We can consider that noise is just a medium throughout the generation process.

SR3 [30] proposed a diffusion super-resolution model which has similar evaluation and training procedures with DDPM. The U-Net in SR3 was redesigned to use a low-resolution (LR) image as guidance to the noise prediction. SR3 concatenates the LR image with Gaussian noise at first step and uses intermediate denoising result in every denoising step, where 2000 steps in total is default in SR3 or IDM [7] models. This conditioning system confirms the pattern predicted by the U-Net which can match the representation of the LR image. Hence, SR3 can generate a super-resolution (SR) image consistent with the LR image. These image transformation diffusion models still bear much the idea of image generation rather than transforming a small image to a high-resolution image [6, 7, 15, 18, 19, 30, 31, 33, 36, 37].

We consider that adding Gaussian noises is just a means

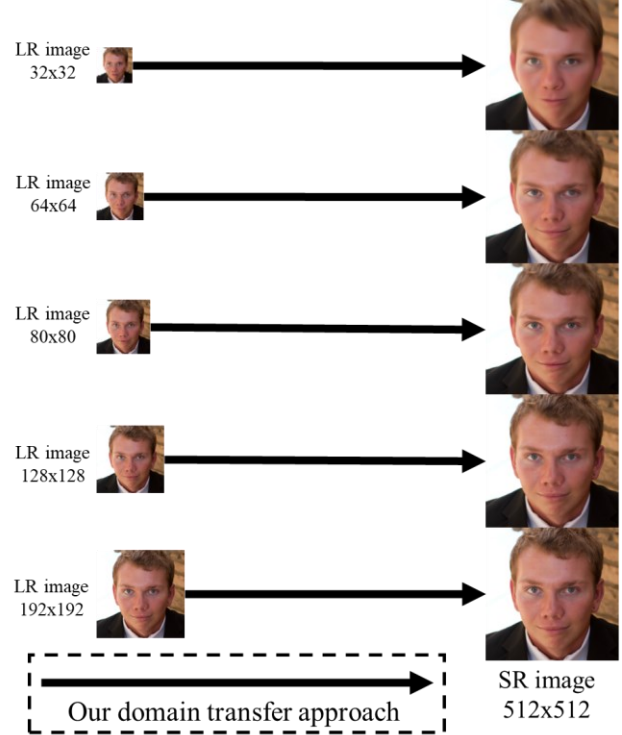


Figure 3. Image super-resolution with our domain transfer method. It can process various input image sizes with only one trained model.

to build a photo-realistic high-resolution image space with reference to an initial noise pattern, and the training procedure is to let the U-Net learn the statistical properties of the training dataset and the statistical differences between time t -stages. While the denoising procedure of diffusion models is to make use of the predicted statistical properties obtained from the trained U-Net (and the derived formulation) to move toward the constructed photo-realistic high-resolution image space. Therefore, we propose our super-resolution approach which shares some concepts of diffusion models but without the use of Gaussian noise at

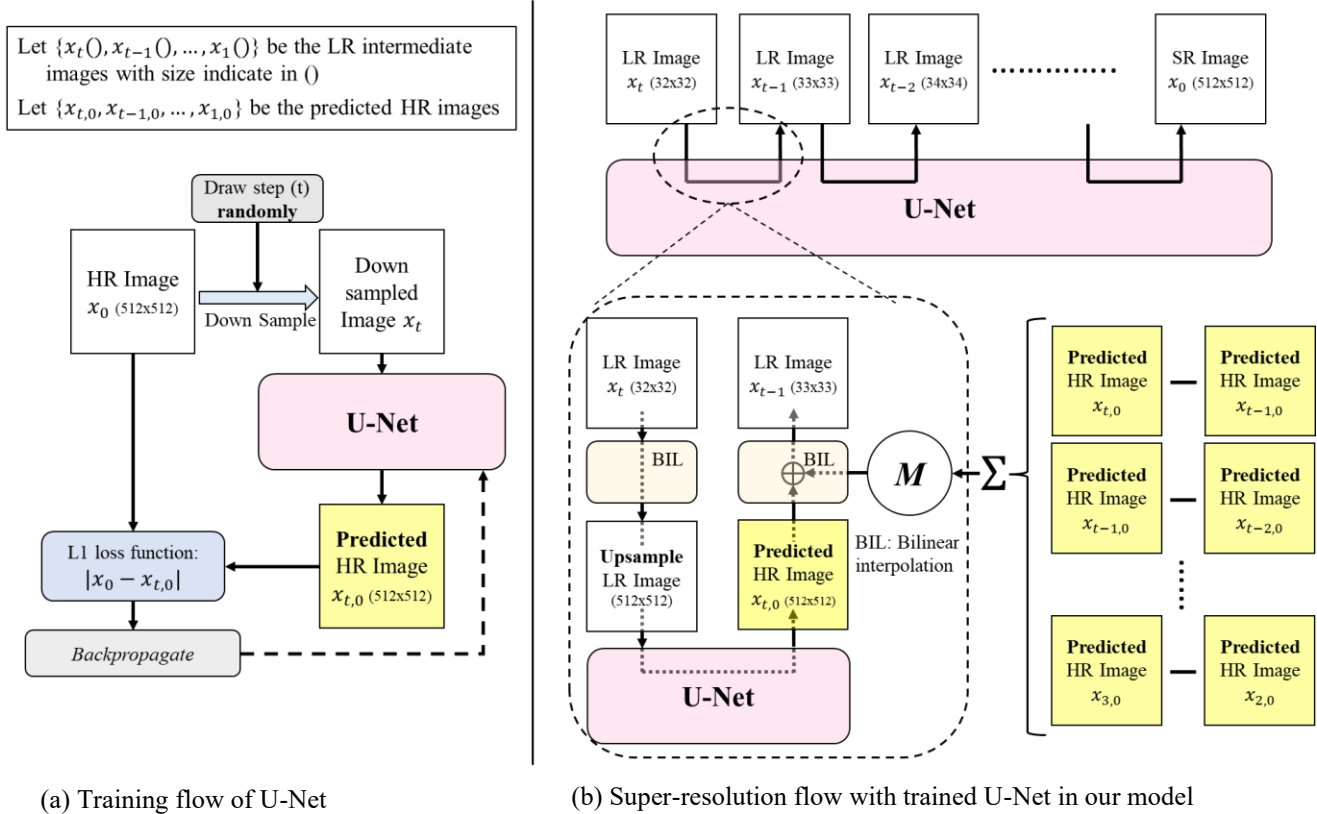


Figure 4. Training and image super-resolution flow of our model

all. We make use of the statistical properties predicted from the trained DNN (for realization just used a trained U-Net) to gradually transfer a LR image to a SR image as shown in Fig.2. Image generation or image super-resolution is done gradually via each scale step as shown in the diagram (indicated by the red arrows).

As verified by our experimental work, just making use of the consecutive reverse process is able to produce super-resolved images with reasonable quality, but the quality is inferior to those produced by Diffusion Models [7, 30]. It is because a Markov chain reverse process may sideway the path which leads to the loss of fidelity. Hence, we relate each step with the LR image in question and introduce an element M , where M acts like an opposite momentum to errors. The super-resolution results are substantially better than the state-of-the art approaches, including Diffusion Models. Details are found below and in our ablation studies.

2. Methodology

In this work, we introduce our novel Domain Transfer in Latent Space (DTLS) framework for image super-resolution based on the concept of iterative domain transfer as shown in Fig. 2. One key advantage of our iterative approach is the flexibility it provides in both input and output resolutions.

As shown in Fig. 3, DTLS can accommodate varying input resolutions, including uncommon sizes like 80×80 or 192×192 pixels. A second advantage of DTLS is its ability to perform extremely large-scale transformations, as it will be demonstrated in our experimental results. In this paper, we utilize face super-resolution as an example application to showcase the effectiveness of our proposed DTLS method.

2.1. Theory

One similar concept between diffusion model and our design is that, both models learn sets of image space from degraded domain to clear domain. The difference is, the degrade domain of diffusion model is achieved by Gaussian noise and our design aims to handle noise (the difference) between various levels of natural image degradation. Diffusion models are carefully designed systems that break down noise adding and denoising into a number of steps, for which they are well-defined with the probabilistic models.

The U-Net actually occupies a big part in the diffusion model, for example, a better design of the U-Net can enhance the performance of image synthesis by the diffusion model [5]. As the U-Net is trained to build a structure for producing the latent image space at various stages via Gaussian noise, it eventually can produce high-resolution

image in the final high-resolution latent domain (making use of the trained parameters). We assume that the U-Net can also be trained and be used to produce intermediate domain results and eventually lead to the final result, with a high quality super-resolved image without involving the mechanism of noise operations. We refer it to as a domain transfer, which transfers a 249x249 image to a 248x248 image say for example, and its reverse for the reverse processing. The transfer has to be small and gradual such that the U-Net is able to accommodate. The fact making this possible is that, as shown in Fig. 2, we have the HR(512x512) and LR(32x32) image pairs available, and in the training, we force (with well-designed loss-functions) to form the weights in the U-net to fulfill our objective to produce high quality HR image in the reverse process.

2.2. Overall Structure

Super-resolution flow

```

Input:  $x_{t=T}$ 
 $M = 0$ 
for  $t = T, T-1, \dots, 1$  do
     $x_{t,0} \leftarrow U(x_t, t)$ 
    if  $t \neq T$  then
         $M = M + x_{t,0} - x_{t-1,0}$ 
     $x_{t-1} \leftarrow D(x_{t-1,0}, t-1) + D(M, t)$ 
return  $x_0$ 

```

Training procedure

```

repeat:
     $t \sim$  Randomly sample from  $\{1 \dots T\}$ 
     $x_0 \sim$  Randomly sampling from Dataset  $\{x_0\}$ 
     $x_t \leftarrow D(x_0, t)$ 
     $x_{t,0} \leftarrow U(x_t, t)$ 
     $Loss \leftarrow |x_{t,0} - x_0|$ 
Backpropagate
Until break

```

Figure 4a shows the training procedure of our model. Similar to diffusion models, the training image x_0 is randomly down sampled to x_t . The U-Net is used to predict a HR image $x_{t,0}$ with any down sampled x_t . A L1 loss function takes x_0 and $x_{t,0}$ to calculate the error to perform backpropagation. By randomly down sample HR images, our U-Net learns the statistical properties of all images $\{x_0\}$ in all degraded image space, from the smallest (ex. 32x32) to the largest (ex. 512x512).

For the super-resolution part as shown as Fig. 4b, the LR image is gradually enlarged with the concept of domain transfer. To achieve domain transfer, the model requires a clear image as guidance, which is the predicted HR image $x_{t,0}$.

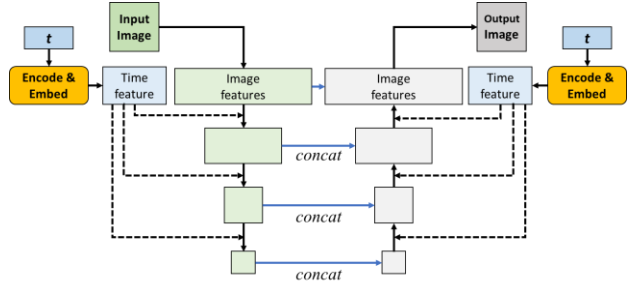


Figure 5. Overall structure of U-Net used in our DTLS, note that t was inputted for guiding the U-Net to produce correct restoration result.

To make use of the input image of smaller size for the U-Net, we firstly apply bilinear interpolation to up sample the LR image to the size of HR image. For instance, as shown in Fig. 3b, the LR image (32x32) is firstly up sampled to 512x512 before inputting to the U-Net. After the prediction, a down sampling with bilinear interpolation will transfer the large image (size:512x512) to x_{t-1} for which the size is 33x33.

Only using this structure, the approach does not work too well. Hence in between the upsampling action and after making the prediction from the U-Net, an element M which is the sum of all previous errors is added (see Section 3.2). This is similar to back projection design [9, 20, 21, 34]. The summation of these inversion errors can be expressed as $\sum_{s=T}^t (x_{s,0} - x_{s-1,0})$, where T is the total transformation steps and t is the current step. Note that at first and second steps, since $x_{t,0}$ and $x_{t-1,0}$ still have not predicted, thus M is equal to zero at these first two steps.

We also denote the training procedure and super-resolution flow in pseudo codes as shown at the beginning of this section, where $D()$ is the down sample operator which includes a down sample and a up sample bilinear interpolation. The purpose of up sample is to make all input images the same size for U-Net operations. The U-Net is represented by $U()$, which aims to predict the HR image $x_{t,0}$. The overall structure of the U-Net is shown as in Fig. 5. Similar to the one in the diffusion model, the U-Net uses timestep t to condition the down sampling and upsampling blocks.

2.3. Error and Momentum

The above procedure is a Markov chain process, meaning that the transfer is between two neighbouring domains, but not other domains. However, the error will accumulate between pairs of domains in the transfer process, which ultimately leads to big error at the final stage and to the final resultant image. Fig.6 shows that, for the first iteration, the U-Net generates a predicted HR image that could slightly deviate from the expected value. When we move further towards the ground truth image x_0 , bigger errors are formed

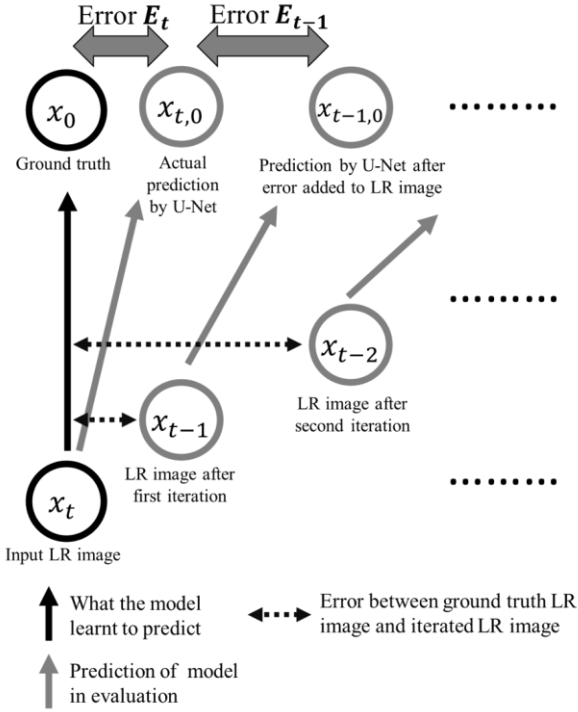


Figure 6. Flow diagram to explain how error accumulates during domain transfer.

due the accumulation. Note that the CNN model was not trained for distorted inputs. It will produce even bigger errors with distorted inputs. This initializes a vicious cycle where the error E_t accumulates all coming iterations.

To address the issue of error accumulation in iterative models, we propose a momentum term M . As the prediction error E accumulates over iterations, we simply add momentum M in the opposite direction. As shown in Fig. 4 and Fig. 7, M is calculated as the sum of previous errors. The change from $x_{t,0}$ to $x_{t-1,0}$ can be obtained by $(x_{t-1,0} - x_{t,0})$ where the change here is considered as error. Therefore, to acquire contrary direction of error, a swap action is taken as $(x_{t,0} - x_{t-1,0})$ and thus M is summation as $\sum_{s=T}^t (x_{s,0} - x_{s-1,0})$.

The physical meaning of momentum is further explained in Fig. 7, as the prediction errors tend to propagate to the model's outputs in the same direction over time (the red arrow moving right), momentum works to cancel out these errors by building up in the opposite direction (the blue arrow moving left). Through this cancellation effect at each iteration, momentum helps control the growth of total error. Additional ablation studies on the impact of momentum are presented in section 3.3. Incorporating this momentum term enables our model to iteratively transform images while mitigating accumulated error artifacts.

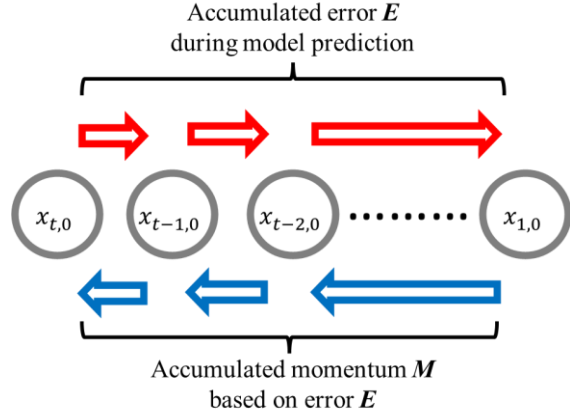


Figure 7. While error E appear between from t to $t-1$, our momentum M can counter in opposite direction.

3. Experimental Results

Dataset To test our DTLS system in face super-resolution, we used FFHQ 1024x1024 dataset which contains 70,000 images [17]. The training image is randomly cropped to the targeted size. Horizontal flip is also used as image augmentation for robustness training.

Implementation details We implemented our design in Py-Torch 1.10.2 with the training on a single NVIDIA RTX3090 (24G VRAM). We chose two common large super-resolution scales for the experiment. The first one is from 16×16 to 128×128, where we applied the U-Net with channel widths of {64, 128, 256, 1024}. The other super-resolution set is 32×32 to 512×512, and the channel widths are {32, 64, 128, 128, 256, 256, 512}. Optimizer AdamW with betas {0.9, 0.999} and eps 1e⁻⁸ were used, and the learning rate was set to 2e⁻⁵. 50K iterations with batch size of 32 and 374K iterations with batch size of 4 were applied on 16 to 128 and 32 to 512 respectively.

3.1. Comparisons with Non-Diffusion Models

While DTLS has the advantage of handling variable input and output resolutions, most state-of-the-art face super-resolution models were designed for single-scale transformations. Therefore, to conduct comparison, we tried the evaluation on three scales: 32×32 to 512×512, 64×64 to 512×512 and 128×128 to 512×512. Two image quality assessment metrics SSIM and PSNR are used for quantitative comparisons. Tab. 1 shows the comparison of SSIM and PSNR of our approach with two state-of-the-art methods, Face-SPARNet [3] and GCFSR [10]. Face-SPARNet makes use of spatial attention network to perform face super-resolution. GCFSR designs a scale-controllable encoder-generator structure to perform face super-resolution

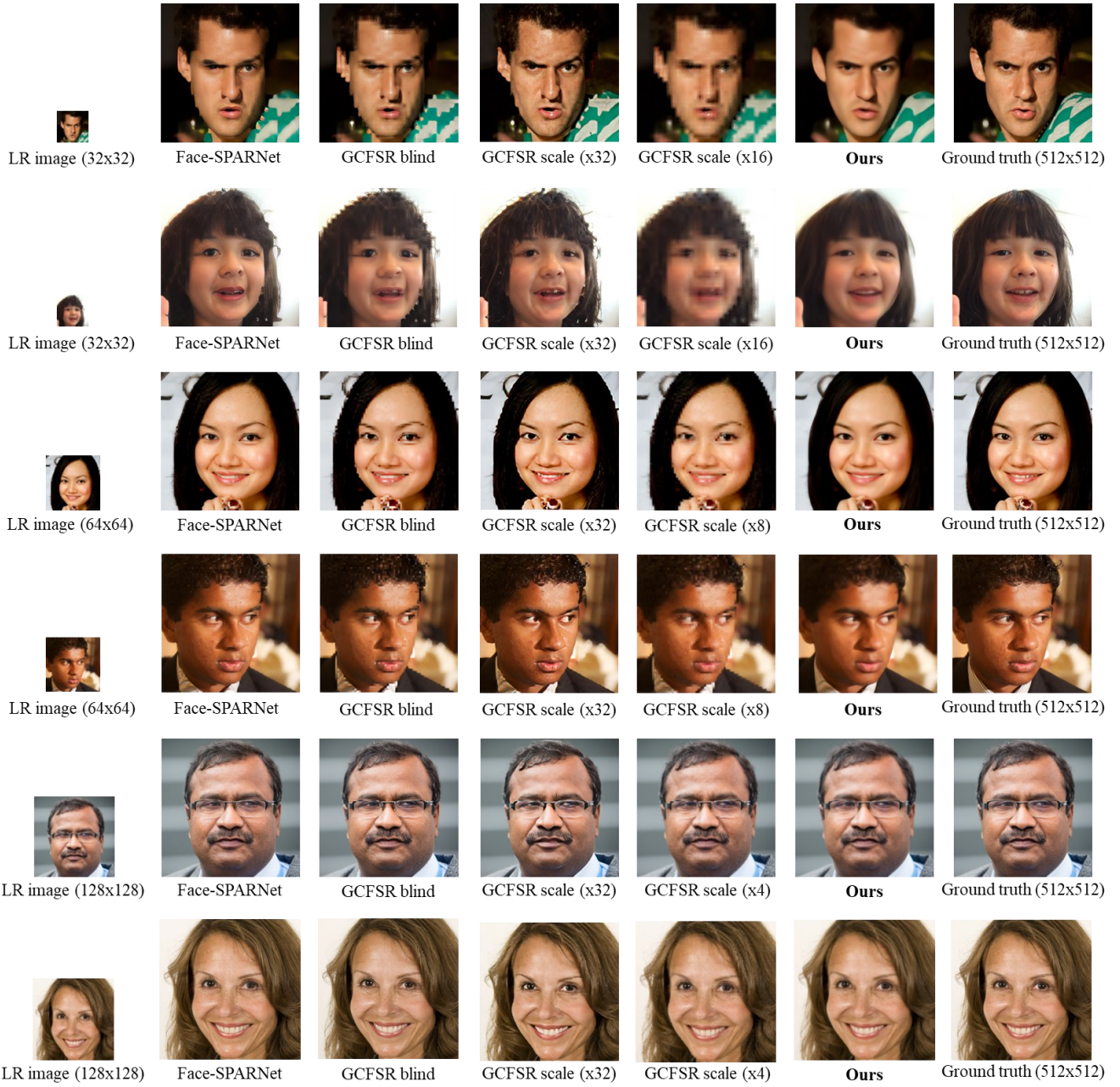


Figure 8. Visual comparison with other SOTA non-diffusion models.

in any enlargement scale. To ensure a fair comparison, we downloaded and used their pre-trained network provided on their project websites with dataset of FFHQ. Visual examples for comparison are also shown in Fig. 8. Our model outperforms both Face-SPARNet and GCFSRs in all super-resolution scales on SSIM and PSNR. This is especially true in extreme scales like 32 to 512 ($\times 16$). I.e., when performing large-scale super-resolution, our DTLS is able to stably and smoothly upsample faces while minimizing artifacts. In contrast, Face-SPARNet and

GCFSR tended to either over-sharpen details or produced under-resolved outputs in these extreme transformation settings. At smaller enlargement scales, with faces closer to ground truth resolution, DTLS still consistently generated images with clear facial details. Overall, DTLS has demonstrated robust and stable performance compared to existing models, especially for the challenging task of high-magnitude super-resolution where originally the accumulation of artifacts poses a significant problem for iterative approaches.

Method (SSIM↑ / PSNR↑)	32→512	64→512	128→512
Face-SPARNet	0.6044 / 21.9249	0.7288 / 26.1935	0.8179 / 29.2282
GCFSR Blind Face Restoration	0.6071 / 21.6363	0.7270 / 25.7160	0.8455 / 29.9659
GCFSR (×32)	0.5818 / 21.2648	0.6581 / 24.2048	0.7282 / 26.5061
GCFSR (×16, ×8, ×4)	0.6431 / 22.8709	0.7528 / 26.8418	0.8747 / 31.3928
Ours	0.7252 / 24.7641	0.8141 / 28.6682	0.8921 / 32.4579

Table 1. Metrics comparison with other SOTA non-diffusion models. Our method performs better on all scales.

3.2. Comparisons with Diffusion Models

To enable comparison between DTLS and diffusion models which perform super-resolution by conditioning the denoising process on Gaussian noise, we focused our evaluation on the two scales where pre-trained diffusion model checkpoints were readily available:

1) 16×16 to 128×128 and 2) 32×32 to 128×128. Since the original publications and model websites for SR3 and IDM only provided pre-trained weights applicable to these resolution ranges, we confined our analysis to evaluating and visualizing results within the same input-output domains for an unbiased comparison. This has limited our tests to relatively small magnification factors, but it still allows us to have a good comparison of our DTLS system with domain transfer approach to the noise-conditioned generation methods employed by diffusion models for face super-resolution.

As shown in Fig. 9, for up sampling from 16×16 to 128×128 (an enlargement factor of ×8), the DTLS continues to stably generate super-resolved results that closely match the structures in the ground truth images. While SR3 and IDM produce high-fidelity images, their outputs do not align as well with the ground truth HR targets compared to DTLS, as evidenced by low SSIM and PSNR scores in Tab. 2. For the 32×32 to 128×128 (×4) case, SR3 is not able to sufficiently leverage the LR image as condition for the guidance and often produced distorted facial features. DTLS more accurately transfers between domains by incrementally shifting through intermediate resolutions, rather than relying on a single noise-conditioned generation step. This allows it to better preserve structural fidelity to the target domain when performing large-scale face super-resolution. While SR3 produces high-quality images in the 16 → 128 case, it is important to note that diffusion-based models like SR3 generates a new image guided by noise rather than explicitly enlarging a degraded input. As discussed previously, this means that the SR outputs from diffusion models may not perfectly produce the target HR images, even they result in photo realistic images. This is evident in Fig. 9, where SR3’s outputs have high fidelity but do not precisely align with the ground truths. On quantitative consistency as shown in Tab. 3, DTLS has obtained images with better consistency and been able to produce SR images that correspond to the LR inputs.

Method (SSIM↑ / PSNR↑)	16→128	32→128
SR3	0.6922 / 23.5806	0.4890 / 18.0262
IDM	0.6426 / 23.0934	0.7465 / 24.0079
Ours	0.7367 / 24.0065	0.8636 / 27.6423

Table 2. Metrics comparison (SSIM/PSNR) with diffusion super-resolution models. Our method performs better on all scales.

Method (Consistency ↓)	16→128	32→128
SR3	0.394	2.439
IDM	0.442	1.597
Ours	0.125	0.648

Table 3. Comparison of consistency, consistency measures MSE ($\times 10^{-5}$) between the LR inputs and the down-sampled SR outputs.

3.1. Ablation Studies

In this section, we focus more on the novelty, momentum M . We have explained the concept of M in Fig. 6, a further exploration is conducted in the following section.

When we firstly applied our iterative image enlargement design, the quality of SR results was not too good, and there were many parts with over-smoothing. We found that the quality of predicted HR image $x_{t,0}$ from U-Net drops with more iterations. Various evidence from our experimental works have shown us the effect in Fig. 6, where the error of prediction accumulated throughout the domain transformation process. This is the reason why we have introduced M , as a stabilizer.

To study the momentum M , we have compared various usages of M , say on 32 → 512 face super-resolution. Note that momentum M does not obtain by training the U-Net. Table 4 shows the results of checking the usefulness of M , where all results were obtained from one pre-trained U-Net. Metrics were measured in SSIM and PSNR. Let us discuss cases with labels (i) to (vi) as shown in Table 4. (i) Without the use of momentum M to reduce restoration errors, it performs the worst among all other situations that make use of M properly. (ii) If we used M for two

Method	SSIM	PSNR
(i) w/o M	0.7110	24.5093
(ii) M w/o accumulation	0.7141	24.5760
(iii) M adding in HR domain	0.7233	24.7508
(iv) Our current design	0.7252	24.7641
(v) w/o degrading M	0.0832	15.9781

Table 4. Metrics comparison of our DTLS in different usages of momentum M .

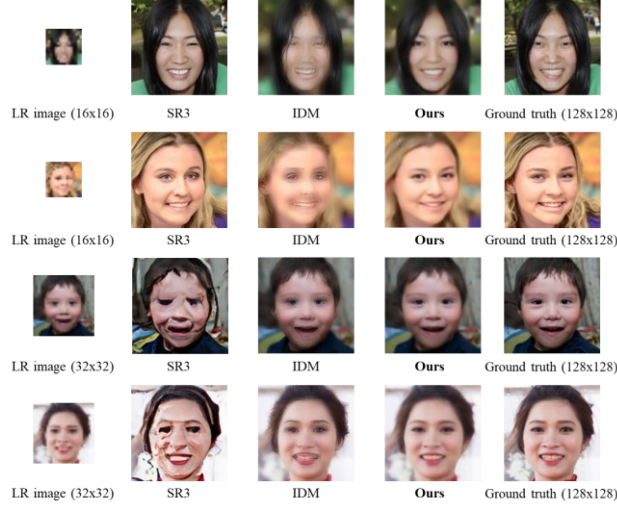


Figure 9. Visual comparison with diffusion faces super-resolution models.

consecutive levels only, which means M no longer accumulates long term previous errors, it only gains 0.003 and 0.067 in SSIM and PSNR and it is still better than those without the use of momentum, but now with almost neglectable improvement. (iii) Adding M in the predicted HR domain image $x_{t,0}$ instead of x_t , (in the LR domain) which indicates that M is no longer needed to be bilinear degraded before (refer to Fig. 4b, M is passing through the bilinear interpolation block): that is instead, M can be added to $x_{t,0}$ since errors are calculated in HR domain ($x_{t,0} - x_{t-1,0}$). However, our study shows that this method has a decrease in quality (-0.0029 SSIM) and (-0.0133 PSNR) compared with our current strategy on the use of momentum. This is because the use of the M after the U-Net prediction cannot let the U-Net to predict a better $x_{t,0}$ with $(x_t + M)$. (iv) This is our current strategy. Our current tactic allows the U-Net to predict the HR image with modulated LR image from the use of M . (v) Lastly, we may degrade M before putting M in the LR image x_t . As mentioned in (iii), previous prediction errors are calculated in HR images, a HR image cannot be added into a LR image without down sampling, otherwise it will distort the domain of the LR image and make DTLS have difficult to make domain transfer properly. This can be seen that both SSIM and



Figure 10. Without degradation of momentum M , the SR result distorted massively (right) compared to proper usage of M (left).

PSNR of (v) have decreased massively. Meanwhile, the visual comparison of (iv) and (v) is shown in Fig. 9. The result of adopting M to our DTLS without down sampling gives huge distortion because the domain transferring process is interrupted.

4. Conclusion

In this work, we introduced our model on Domain Transfer in Latent space (DTLS) for super-resolution imaging, which demonstrates the potential for noiseless iterative design for image-to-image translation tasks. Leveraging the concept of domain shifting across intermediate representations and guided by an error-correction momentum term M , DTLS successfully overcomes issues of error accumulation. In our experiments on face super-resolution, DTLS outperformed state-of-the-art methods across all scales of magnification in super-resolution imaging, validating its ability to handle highly flexible, multi-scale transformations.

Super-resolution is suggested in this paper as it is a commonly ill-posed problem in image-to-image transformation. The exploration of our model should not end here. Our proposed novel approach could also be extended to other image transformation tasks. We recommend tasks such as low-light image enhancement, deblurring, denoising, inpainting, etc. The goal is for DTLS to serve as a versatile image transformation architecture applicable to a wide variety of restoration and enhancement problems through further research.

More broadly, our framework opens new opportunities beyond existing approaches by enabling general any-input to any-output flexibility. For instance, it may allow freely adjusting image properties like brightness over a continuous range for low-light enhancement. We hope our work inspires further research on domain transfer paradigms. With continued development, iterative domain transfer models may become a universally applicable approach for image transformation tasks. Our model presents just a starting point, and more advances are still needed to unlock the full promise of this new direction.

ACKNOWLEDGMENT

This work is partly supported by the Caritas Institute of Higher Education (1SG200206) and UGC Grant (UGC/FDS11/E05/22) of the Hong Kong Special Administrative Region.

References

[1] Arpit Bansal, Eitan Borgnia, Hong-Min Chu, Jie S Li, Hamid Kazemi, Furong Huang, Micah Goldblum, Jonas Geiping, and Tom Goldstein. Cold diffusion: Inverting arbitrary image transforms without noise. *arXiv preprint arXiv:2208.09392*, 2022.

[2] Fan Bao, Shen Nie, Kaiwen Xue, Yue Cao, Chongxuan Li, Hang Su, and Jun Zhu. All are worth words: A vit backbone for diffusion models. In *Proceedings of the IEEE/CVF Conference on Computer Vision and Pattern Recognition*, pages 22669–22679, 2023.

[3] Chaofeng Chen, Dihong Gong, Hao Wang, Zhifeng Li, and Kwan-Yee K Wong. Learning spatial attention for face super-resolution. *IEEE Transactions on Image Processing*, 30:1219–1231, 2020.

[4] Florinel-Alin Croitoru, Vlad Hondu, Radu Tudor Ionescu, and Mubarak Shah. Diffusion models in vision: A survey. *IEEE Transactions on Pattern Analysis and Machine Intelligence*, 2023.

[5] Prafulla Dhariwal and Alexander Nichol. Diffusion models beat gans on image synthesis. *Advances in neural information processing systems*, 34:8780–8794, 2021. 2, 4

[6] Ben Fei, Zhaoyang Lyu, Liang Pan, Junzhe Zhang, Weidong Yang, Tianyue Luo, Bo Zhang, and Bo Dai. Generative diffusion prior for unified image restoration and enhancement. In *Proceedings of the IEEE/CVF Conference on Computer Vision and Pattern Recognition*, pages 9935–9946, 2023.

[7] Sicheng Gao, Xuhui Liu, Bohan Zeng, Sheng Xu, Yanjing Li, Xiaoyan Luo, Jianzhuang Liu, Xiantong Zhen, and Baochang Zhang. Implicit diffusion models for continuous super-resolution. In *Proceedings of the IEEE/CVF Conference on Computer Vision and Pattern Recognition*, pages 10021–10030, 2023.

[8] Ian Goodfellow, Jean Pouget-Abadie, Mehdi Mirza, Bing Xu, David Warde-Farley, Sherjil Ozair, Aaron Courville, and Yoshua Bengio. Generative adversarial nets. In *Advances in Neural Information Processing Systems*. Curran Associates, Inc., 2014.

[9] Muhammad Haris, Gregory Shakhnarovich, and Norimichi Ukita. Deep back-projection networks for super-resolution. In *Proceedings of the IEEE conference on computer vision and pattern recognition*, pages 1664–1673, 2018.

[10] Jingwen He, Wu Shi, Kai Chen, Lean Fu, and Chao Dong. Gcfsr: a generative and controllable face super resolution method without facial and gan priors. In *Proceedings of the IEEE/CVF Conference on Computer Vision and Pattern Recognition*, pages 1889–1898, 2022.

[11] Jonathan Ho, Ajay Jain, and Pieter Abbeel. Denoising diffusion probabilistic models. *Advances in neural information processing systems*, 33:6840–6851, 2020.

[12] Jonathan Ho, Chitwan Saharia, William Chan, David J Fleet, Mohammad Norouzi, and Tim Salimans. Cascaded diffusion models for high fidelity image generation. *The Journal of Machine Learning Research*, 23(1):2249–2281, 2022.

[13] Xiaodan Hu, Mohamed A Nael, Alexander Wong, Mark Lamm, and Paul Fieguth. Runet: A robust unet architecture for image super-resolution. In *Proceedings of the IEEE/CVF Conference on Computer Vision and Pattern Recognition Workshops*, pages 505–507, 2019. 4

[14] Chun-Chuen Hui, Wan-Chi Siu, Ngai-Fong Law, and H Anthony Chan. Intelligent painter: New masking strategy and self-referencing with resampling. In *2023 24th International Conference on Digital Signal Processing (DSP)*, pages 1–5. IEEE, 2023.

[15] Yitong Jiang, Zhaoyang Zhang, Tianfan Xue, and Jinwei Gu. Autodir: Automatic all-in-one image restoration with latent diffusion. *arXiv preprint arXiv:2310.10123*, 2023.

[16] Younghyun Jo, Sejong Yang, and Seon Joo Kim. Investigating loss functions for extreme super-resolution. In *Proceedings of the IEEE/CVF conference on computer vision and pattern recognition workshops*, pages 424–425, 2020.

[17] Tero Karras, Samuli Laine, and Timo Aila. A style-based generator architecture for generative adversarial networks. In *Proceedings of the IEEE/CVF conference on computer vision and pattern recognition*, pages 4401–4410, 2019.

[18] Guangyuan Li, Wei Xing, Lei Zhao, Zehua Lan, Jiakai Sun, Zhanjie Zhang, Quanwei Zhang, Huaizhong Lin, and Zhijie Lin. Self-reference image super-resolution via pre-trained diffusion large model and window adjustable transformer. In *Proceedings of the 31st ACM International Conference on Multimedia*, pages 7981–7992, 2023.

[19] Haoying Li, Yifan Yang, Meng Chang, Shiqi Chen, Huajun Feng, Zhihai Xu, Qi Li, and Yueting Chen. Srdiff: Single image super-resolution with diffusion probabilistic models. *Neurocomputing*, 479:47–59, 2022.

[20] Zhi-Song Liu, Li-Wen Wang, Chu-Tak Li, and Wan-Chi Siu. Image super-resolution via attention based back projection networks. In *IEEE International Conference on Computer Vision Workshop (ICCVW)*, 2019.

[21] Zhi-Song Liu, Li-Wen Wang, Chu-Tak Li, and Wan-Chi Siu. Hierarchical back projection network for image super-resolution. In *Proceedings of the IEEE/CVF conference on computer vision and pattern recognition workshops*, pages 2041–2050, 2019.

[22] Zhi-Song Liu, Wan-Chi Siu, and Yui-Lam Chan. Features guided face super-resolution via hybrid model of deep learning and random forests. *IEEE Transactions on Image Processing*, 30:4157–4170, 2021.

[23] Zhi-Song Liu, Wan-Chi Siu, and Li-Wen Wang. Variational autoencoder for reference based image super-resolution. In *Proceedings of the IEEE/CVF Conference on Computer Vision and Pattern Recognition*, pages 516–525, 2021.

[24] Cheng Lu, Yuhao Zhou, Fan Bao, Jianfei Chen, Chongxuan Li, and Jun Zhu. Dpm-solver: A fast ode solver for diffusion probabilistic model sampling in around 10 steps. *Advances in Neural Information Processing Systems*, 35:5775–5787, 2022.

[25] Cheng Lu, Yuhao Zhou, Fan Bao, Jianfei Chen, Chongxuan Li, and Jun Zhu. Dpm-solver++: Fast solver for guided sampling of diffusion probabilistic models. *arXiv preprint arXiv:2211.01095*, 2022.

